IOP Publishing Plasma Sources Science and Technology
Plasma Sources Sci. Technol. 31 (2022) 045016 (8pp) https://doi.org/10.1088/1361-6595/ac54c0

# Cross sections for vibrational excitation and dissociative recombination of the $CF_3^+$ ion in collisions with low-energy electrons

**Xianwu Jiang[1], Hainan Liu[2,*], Ya Zhang[1], Wei Jiang[3], Mehdi Ayouz[4,*] and Viatcheslav Kokoouline[5]**

[1] Department of Physics, Wuhan University of Technology, Wuhan 430074, People's Republic of China
[2] Department of Basic Courses, Naval University of Engineering, Wuhan 430033, People's Republic of China
[3] School of Physics, Huazhong University of Science and Technology, Wuhan 430074, People's Republic of China
[4] Université Paris-Saclay, CentraleSupélec, Laboratoire de Génie des Procédés et Matériaux, 91190, Gif-sur-Yvette, France
[5] Department of Physics, University of Central Florida, 32816, Florida, United States of America

E-mail: lhn327jiayou@163.com and mehdi.ayouz@ecp.fr

Received 8 December 2021, revised 22 January 2022
Accepted for publication 14 February 2022
Published 10 May 2022

**Abstract**

Cross sections for the vibrational excitation and dissociative recombination (DR) of the $CF_3^+$ ion in collisions with electrons at low scattering energies are computed using a previously-developed approach combining the normal mode approximation for the vibrational states of the target ion and the UK *R*-matrix code for the evaluation of the scattering matrices at fixed geometries. The obtained cross section for the DR shows excellent agreement with the experimental data from the ASTRID storage ring. Thermally-averaged rate coefficients are obtained from the cross sections for temperatures 10–3000 K.

Keywords: dissociative recombination, vibrational excitation, *R*-matrix method

Supplementary material for this article is available online

(Some figures may appear in colour only in the online journal)

## 1. Introduction

Carbon tetrafluoride ($CF_4$) is one of the most widely used etching gases in microelectronic manufacturing. It serves as a source of reactive species, in particular F atoms reacting with the substrate surface, and positive ionic fragments, which play a critical role in physically bombarding the substrate surface. The investigation into various physical and chemical reactions occurring in $CF_4$ plasma is thus of a considerable technological interest [1]. Electron-induced dissociative ionization of $CF_4$,

$$e^- + CF_4 \rightarrow 2e^- + CF_3^+ + F, \quad (1)$$

produces $CF_3^+$ (trifluoromethyl cation) with a threshold energy of 16 eV and a fast rate coefficient of $9.36 \times 10^{-8} \exp(-20.4/T_e)$ cm$^3$ s$^{-1}$ ($T_e$ is the electron temperature) [2]. The species could also be generated by the ionization of $CF_3$ radicals in $CF_4$ plasma

$$e^- + CF_3 \rightarrow 2e^- + CF_3^+, \quad (2)$$

with a threshold of 10.4 eV and a rate of $8 \times 10^{-9} \exp(-12.2/T_e)$ cm$^3$ s$^{-1}$ [2]. Other types of collisions, for instance electron-induced dissociation of $CF_4$ and $CF^+(CF_2^+)$–$CF_4$, may also yield $CF_3^+$ with slower rates or/and larger thresholds.

The cross section for producing $CF_3^+$ by ionization of $CF_4$ is one order of magnitude larger than those for $C^+$, $F^+$, $CF^+$, and $CF_2^+$. The $CF_3^+$ ion was identified as the dominant positive ion, by mass spectrometry [3] and by theory [4], in pure

* Authors to whom any correspondence should be addressed.

 © 2022 IOP Publishing Ltd Printed in the UK

$CF_4$ plasmas and in mixture plasma of $CF_4$ with, for instance, Ar [5], $O_2$ [6, 7], and $N_2$ [8], as well as in some alternative fluorocarbon plasmas $CF_3X$ ($X$ = Cl, Br, H, I) [9, 10]. Dissociative recombination (DR) of $CF_3^+$ with low-energy electrons proceeds towards the following dissociation channels

$$e^- + CF_3^+ \rightarrow CF_2 + F, \quad (3)$$

$$CF + 2F. \quad (4)$$

The branching ratio for the two channels was determined in the ASTRID storage ring experiment to be 80 ± 10% and 20 ± 10%, respectively [11]. CF and $CF_2$ radicals in the plasma contribute to the polymerization of fluorocarbon on the substrate surface, which impacts significantly the etching rate and selectivity [12]. Experimental investigations [13, 14] indicate that electron-impact dissociation of $CF_4$ producing CF and $CF_2$ accounts for only about 5% and 10% of the total rate. The DR process, and not the negative–positive ion mutual recombination, is the primary loss mechanism of $CF_3^+$ in a low-temperature plasma, particularly at low pressure. Thus, DR of $CF_3^+$ must be considered as one of the major formation routes of CF and $CF_2$ radicals. The cross section of the process is essential data for adequately understanding, characterizing, and modelling the $CF_4$ plasma [15].

$CF_3^+$ is generally included in $CF_4$ plasma modeling for its abundance. However, the $CF_3^+$ DR was rarely taken into account due to missing information about the cross section of this process [4]. The rate coefficient for this process was estimated in 1976 [16] to be $3.95 \times 10^{-9} T_e^{-1/2} T_i^{-1}$ cm$^3$ s$^{-1}$, where $T_e$ and $T_i$ are in units of eV and represent the electron and $CF_3^+$ temperatures. The formula yields the rate coefficient of $9.6 \times 10^{-7}$ cm$^3$ s$^{-1}$ for a 300 K plasma. The value was used in several studies [4, 17] until 2004, when the value of $2.8 \pm 0.8 \times 10^{-7}$ cm$^3$ s$^{-1}$ at 300 K, about a factor of three smaller than the above one, was measured using a flowing afterglow Langmuir probe-mass spectrometer apparatus [18]. A similar value of $2.6 \times 10^{-7}$ cm$^3$ s$^{-1}$ at 300 K was obtained from the DR cross section measured in the ASTRID storage ring experiment two years later [11]. A further measurement of the rate coefficient was performed by another FALP experiment in 2013 [19], which produced the value of $3.1 \pm 0.9 \times 10^{-7}$ cm$^3$ s$^{-1}$.

No theoretical study of the $CF_3^+$ DR process and the corresponding cross sections have been reported so far. This might partially be attributed to the complexity and difficulty in theoretically modeling the DR process in polyatomic ions. To cross check the experimental measurements and understand the mechanism of the process, a theoretical computation of the $CF_3^+$ DR cross section and the rate coefficient is desirable. The present study is devoted to a theoretical description of the process. The approach was initially developed in 2013 for the treatment of DR in $HCO^+$ and $N_2H^+$ [20, 21] and has been successfully applied to several molecular ions, such as $BF_2^+$ [22], $CH_2NH_2^+$ [23], $NH_2CHOH^+$ [24].

The article is organized in the following way. In section 2, we describe the structure of $CF_3^+$, details of the present scattering calculations, and the general theoretical approach for modeling the DR in $CF_3^+$. The obtained cross sections and rate coefficients are given in section 3. The application of the current theoretical cross sections in Monte Carlo plasma modeling for etching are discussed in section 4. Section 5 concludes the article.

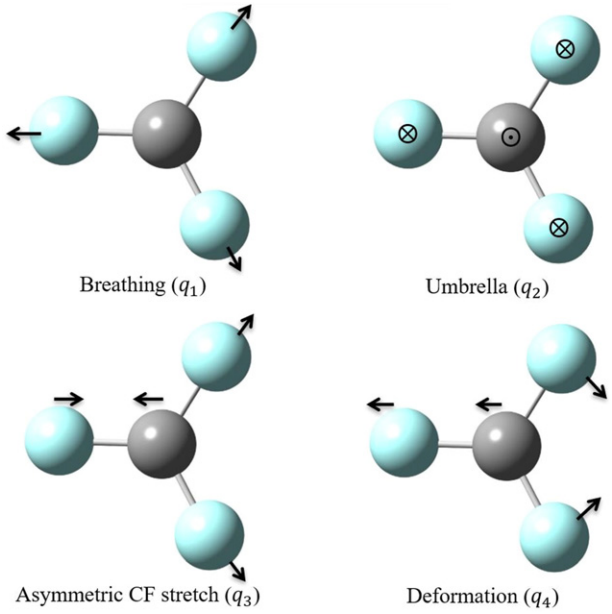


**Figure 1.** Normal modes of $CF_3^+$. Arrows indicate displacement directions of the four atoms when the corresponding modes change. ⊗ and ⊙ represent inward and outward displacements perpendicular to the molecular plane.

## 2. Theoretical approach

### *2.1. Properties of the $CF_3^+$ ion and the scattering calculation*

$CF_3^+$ in the equilibrium geometry has a trigonal planar structure with the C atom at the centre. It belongs to the $D_{3h}$ point group with a C–F bond length of 1.2272 Å [25], with a closed electronic shell in the ground electronic state with the following electronic configuration:

$$X^2A_1' : 1e'^4 1a_1'^2 2a_1'^2 3a_1'^2 2e'^4 4a_1'^2 3e'^4 1a_2''^2 4e'^4 1e''^4 1a_2'^2.$$

The normal mode approximation is used to characterize its lowest vibrational states. The molecular vibration is split into different normal modes where all the nuclei vibrate about their equilibrium position at a certain frequency. As in previous studies [23, 24], dimensionless normal coordinates $q_i$ [26] are employed to characterize displacements from the equilibrium geometry along each normal mode $i$. The normal modes are asymmetric breathing ($A'_1$), umbrella ($A''_2$), asymmetric CF stretching ($E'$), and deformation ($E'$). The corresponding harmonic normal mode frequencies and coordinates will be referred to below as $\omega_1, \omega_2, \omega_3, \omega_4$ and $q_1, q_2, q_3, q_4$. Displacements along the four modes are displayed in figure 1.

We used the MOLPRO [27] package for the electronic structure and normal mode frequency calculations of $CF_3^+$ near its equilibrium geometry. The 6-311G* basis set is used to construct the Hartree–Fock (HF) orbitals of $CF_3^+$ in abelian subgroup $C_s$. The geometry of $CF_3^+$ was optimized using the complete active space self-consistent field method with the HF orbitals. The inner 14 core electrons were frozen, and the

remaining 18 electrons were freely distributed in the CAS consisting of nine $a'$ and four $a''$ orbitals in the $C_s$ group. The optimized C–F bond distance was then used as the distance of the equilibrium geometry in the subsequent frequency calculations. Table 1 summarizes the computed bond length and vibrational frequencies and compares them with the available experimental and theoretical results. The obtained frequencies are in good agreement with the experiments, as seen from the table. The matrix of transformation from Cartesian to normal mode coordinates is obtained in the frequency calculation and used to construct the input geometry for the $e^-$–$CF_3^+$ scattering calculations.

We carried out the scattering calculations using the UK *R*-matrix code [31] and the Quantemol-N interface [32]. The calculation was performed in $C_s$ symmetry and the target $CF_3^+$ ion was assumed to be in its ground electronic state. The ground electronic configuration in $C_s$ is written as

$$X^2A' : 1 - 10a'^2 1a''^2 11 - 12a'^2 2 - 3a''^2 13a'^2.$$

It is worth noting that the horizontal reflection plane $\sigma_h$ for umbrella mode is the vertical reflection plane $\sigma_v$ in $D_{3h}$ symmetry. The ground electronic configuration for umbrella mode is different and turns out to be

$$X^2A' : 1a'^2 1a''^2 2 - 5a'^2 2a''^2 6 - 7a'^2 3a''^2 8 - 9a'^2 4a''^2 10a'^{25} - 6a''^2.$$

For consistency with the structure calculations of the normal modes, the 6-311G* basis set was used in the scattering calculations for the ground HF orbitals. Wave functions of the target's electronic states are computed using the CAS configuration interaction (CAS-CI) method with those HF orbitals. To make the *R*-matrix calculation computationally tractable in the CI model, we freeze the 14 electrons in the seven inner core orbitals and keep the residual 18 electrons in a CAS consisting of 11 orbitals: $8 - 10a'1a''11 - 12a'2 - 3a''13a'4a''14a'$ for the breathing, asymmetric CF stretching, and deformation modes and the $6 - 7a'3a''8 - 9a'4a''10a'5 - 6a''11 - 12a'$ orbitals for the umbrella mode, referred to as CAS(18, 11). We use an *R*-matrix sphere radius of 14 bohrs and continuum Gaussian-type orbitals with partial waves $l \leqslant 4$. All the electronic states generated by the CAS-CI method below 15 eV were included in the close-coupling expansion to construct the total wave function. In the *R*-matrix scattering calculation, we obtained fixed-geometry reactance matrix $\hat{K}(q_i)$ (*K*-matrix) for the collisional system, *i* being the index of the $CF_3^+$ normal modes. The *K*-matrix is used to compute the scattering matrix $\hat{S}(q_i)$.

The eigenphase sums derived from the *K*-matrix of $^2A'$ and $^2A''$ symmetry of the $e^-$–$CF_3^+$ system at the $CF_3^+$ equilibrium geometry and for displacements $q_i = 1$ (dimensionless) along the breathing, umbrella, asymmetric CF stretching and deformation normal modes, are exhibited in figure 2. The variation of the eigenphase sums is smooth for the four normal modes over a scattering energy below roughly 7 eV. Sharp peaks representing Rydberg states attached to the excited electronic states of the ion appear at higher energies. The scattering matrix is thus weakly energy-dependent below 7 eV. For a scattering energy below the first excited state, only the ground electronic state of $CF_3^+$ is open for ionization. Therefore, the dimension of the fixed-geometry scattering matrix stays the same at low scattering energy. From the physical point of view, the smooth eigenphase sums at low energy means there is no low-lying repulsive dissociative states of the neutral molecule crossing the PES of the ground electronic state of the ion near its equilibrium geometry. Therefore, the indirect DR mechanism is dominant at low scattering energies, roughly below 7 eV in the present case.

### 2.2. Dissociative recombination formulas

Here, we just outline the major ideas of the theoretical model because the formalism has been derived and described earlier [20, 21]. The model starts with the following assumptions: (i) the rotational structure of the target ion is ignored, leading to a cross section without rotational resonances. Indeed, such resonances are unresolved in experimental measurements since the target ions are generally in rotationally excited states. Moreover, it is justified for $CF_3^+$ because it has no permanent dipole moment due to its symmetry. (ii) cross section is averaged over autoionizing rovibrational resonances, leading to a constant probability of electronic capture [33]. (iii) autoionization lifetimes of the rovibrational resonances are assumed to be much longer than the predissociation lifetime, i.e. the scattering energy is quickly transferred to the vibrational motion of the target ion if the incident electron is trapped by a rovibrational Rydberg resonance state. The assumption suggests that the predissociation is dominant if the electron scattering energy is lower than the ionization threshold. (iv) The vibration of the molecular ion is described by the harmonic approximation.

Performing the vibrational frame transformation based on the (i)–(iv) assumptions, we obtain the scattering matrix $\hat{S}(q_i)$ that can describe the vibrational excitation (VE). The formula for the VE cross sections for each mode is

$$\sigma_i^{\mathrm{VE}}(E_{\mathrm{el}}) = \frac{\pi\hbar^2}{4mE_{\mathrm{el}}} g_i \sum_{ll'\lambda\lambda'} \left| \frac{\partial S_{l'\lambda',l\lambda}(q_i)}{\partial q_i} \right|^2 \Theta(E_{\mathrm{el}} - \hbar\omega_i), \quad (5)$$

where $m$ and $E_{\mathrm{el}}$ specify the electron mass and the electron scattering energy and $g_i$ is degeneracy of the normal mode $i$. The asymmetric CF stretching and deformation modes are doubly degenerate. $S_{l'\lambda',l\lambda}$ is an element of the fixed-nuclei *S*-matrix for the $e^-$–$CF_3^+$ scattering with $l'\lambda', l\lambda$ representing the initial and final partial waves of the scattering electron: $l$ being the electron angular momentum and $\lambda$ its projection on the molecular axis. The Heaviside step function $\Theta(E_{\mathrm{el}} - \hbar\omega_i)$ equals to 1 when $E_{\mathrm{el}}$ exceeds $\hbar\omega_i$, otherwise 0. Physically, this means the incident electron can excite the ion only if its energy is above the VE threshold. The formula agrees with the general propensity rule: the vibrational (de-)excitation process with a change of one quanta ($\Delta\nu = 1$) in each normal mode is dominant over other (de-)excitation processes. (De-)excitation cross sections for $\Delta\nu \geqslant 2$ in each mode are not considered in this theoretical model. In the present study, the electron could thus only be captured into the first excited vibrational state in each mode as we treat the $CF_3^+$ ion in its ground vibrational level.

**Table 1.** The C–F bond length and vibrational frequencies of $CF_3^+$ obtained in this study and compared with previous experimental and theoretical results. $\omega_1$, $\omega_2$, $\omega_3$ and $\omega_4$ are the frequencies of the breathing, umbrella, asymmetric CF stretching, and deformation modes, respectively.

| | Symmetry | This work | Exp. | Y. Pak *et al*. [25] |
|---|---|---|---|---|
| C–F distance (Å) | | 1.2305 | — | 1.2272 |
| $\omega_1$ ($cm^{-1}$) | $A_1'$ | 1038.15 | 994 ± 16 [28] | 1044 |
| $\omega_2$ ($cm^{-1}$) | $A_2'$ | 829.34 | 809 ± 14 [28] | 813 |
| $\omega_3$ ($cm^{-1}$) | $E'$ | 1678.65 | 1662.4 [29], 1667 [30] | 1683 |
| $\omega_4$ ($cm^{-1}$) | $E'$ | 609.09 | — | 593 |

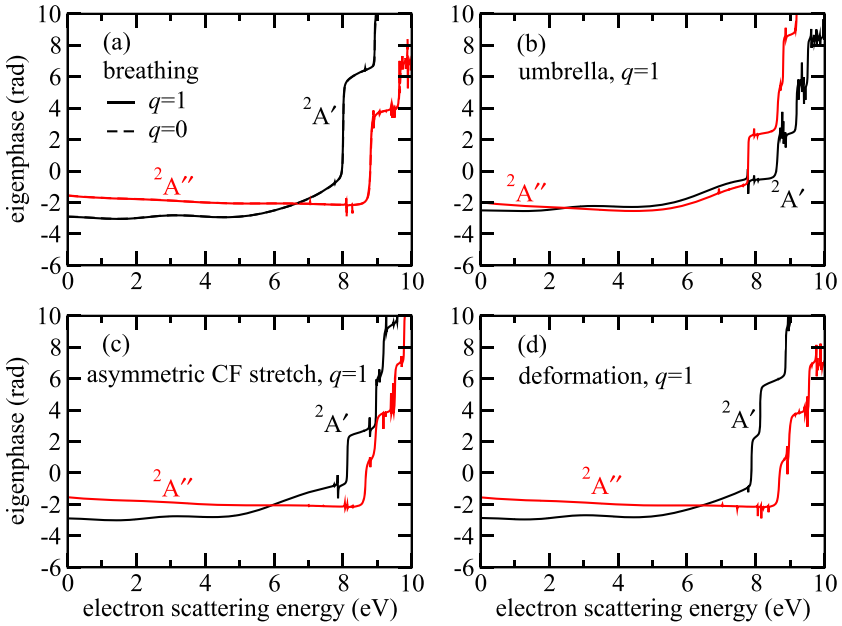


**Figure 2.** Eigenphase sums as a function of electron scattering energy for (a) the equilibrium geometry and $q = 1$ displacement along the breathing coordinate and the same displacements $q = 1$ along (b) the umbrella, (c) asymmetric CF stretching, and (d) deformation coordinates. The black and red curves correspond to $^2A'$ and $^2A''$ symmetry of the $e^-$–$CF_3^+$ scattering wave functions. Note that the eigenphase sum at $q = 1$ is on the top of the curve at $q = 0$ for breathing mode.

When the electron scattering energy is lower than the first excited vibrational level of a particular mode, the incident electron, if it excites this vibrational mode, is captured into an autoionizing vibrational resonance associated with the excited vibrational level, which leads to further VE of the target ion and, in the end, to the dissociation of the formed neutral molecule. Correspondingly, the DR cross section is given by

$$\sigma^{\mathrm{DR}}(E_{\mathrm{el}}) = \frac{\pi\hbar^2}{4mE_{\mathrm{el}}}\sum_i g_i \sum_{ll'\lambda\lambda'}\left|\frac{\partial S_{l'\lambda',l\lambda}(q_i)}{\partial q_i}\right|^2 \Theta(\hbar\omega_i - E_{\mathrm{el}}). \quad (6)$$

The sum in the above expression runs over all the normal modes $i$: breathing, umbrella, "the doubly degenerate" to asymmetric CF stretch and deformation. To evaluate the derivative of the $S$-matrix with respect to the normal mode coordinates $\frac{\partial S_{l'\lambda',l\lambda}(q_i)}{\partial q_i}$, the $S$-matrix is computed for two values of $q_i = 0.01$ and $q_i = 0.1$, while keeping the other normal mode coordinates fixed at equilibrium.

## 3. Cross sections and rate coefficients

For convenience, a quantity $P_i$ is introduced in the form of

$$P_i = \frac{g_i}{2}\sum_{ll'\lambda\lambda'}\left|\frac{\partial S_{l'\lambda',l\lambda}(q_i)}{\partial q_i}\right|^2, \quad (7)$$

to represent the VE probability of the normal mode $i$. The computed probabilities shown in figure 3 are weakly energy-dependent and approximately linear functions of the electron scattering energy. Therefore, they could be fitted with a linear function by $P_i = a_i E_{\mathrm{el}} + b_i$. Table 2 lists fitted parameters $a_i$ and $b_i$ for each normal mode.

The fitted probabilities are then used to compute the VE and DR cross sections by

$$\sigma_i^{\mathrm{VE}}(E_{\mathrm{el}}) = \frac{\pi\hbar^2}{2mE_{\mathrm{el}}} P_i(E_{\mathrm{el}})\Theta(E_{\mathrm{el}} - \hbar\omega_i), \quad (8)$$

and

$$\sigma^{\mathrm{DR}}(E_{\mathrm{el}}) = \frac{\pi\hbar^2}{2mE_{\mathrm{el}}}\sum_{i=1}^{4} P_i(E_{\mathrm{el}})\Theta(\hbar\omega_i - E_{\mathrm{el}}). \quad (9)$$

**Table 2.** Coefficients of the curve fitting function for excitation probability. Energy is assumed to be in Hartree. $a_i$ are in units of 1/Hartree and $b_i$ are dimensionless.

| Mode | $P_1$ | $P_2$ | $P_3$ | $P_4$ |
|---|---|---|---|---|
| $a_i$ | $2.371 \times 10^{-2}$ | $3.488 \times 10^{-1}$ | $7.282 \times 10^{-1}$ | $8.425 \times 10^{-1}$ |
| $b_i$ | $9.043 \times 10^{-4}$ | $3.280 \times 10^{-1}$ | $8.069 \times 10^{-2}$ | $1.711 \times 10^{-1}$ |

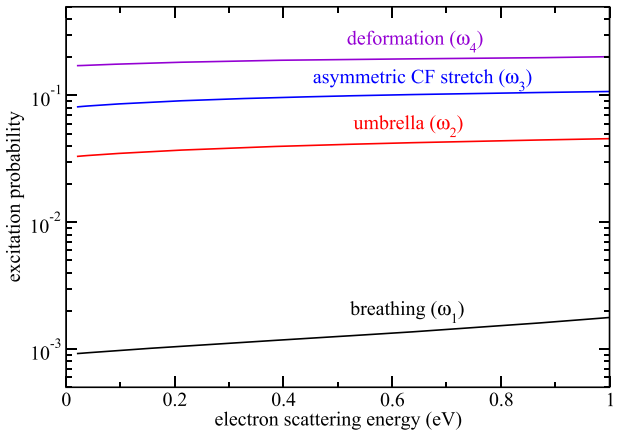


**Figure 3.** Excitation probabilities for each normal mode computed by equation (7).

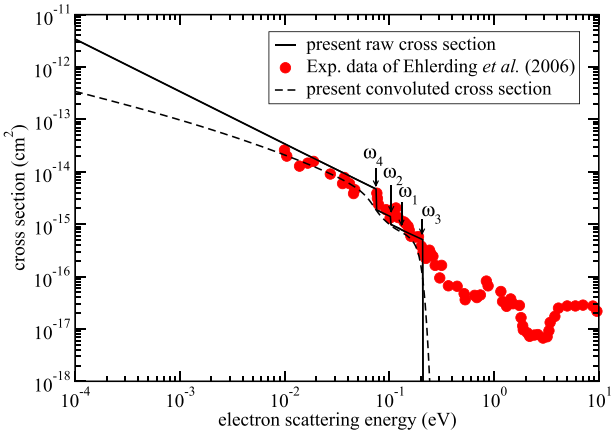


**Figure 4.** Comparisons between the present raw theoretical cross section (black solid curve), the cross section convoluted with experimental distributions over electronic velocities (black dashed curve), and the experimental measurements by Ehlerding *et al* (red solid dot) [11]. The vibrational thresholds corresponding to $\hbar\omega_i$ for the four normal modes are indicated by arrows.

Figure 4 displays the computed DR cross sections (black solid curve). For energies $E_{\rm el}$ below the lowest vibrational threshold $\hbar\omega_4$ (deformation), the cross section obeys the Wigner's law [34] as a smooth function inversely proportional to the electron scattering energy. At higher energies, it drops at the vibrational threshold of each normal mode. Experimental values from the ASTRID storage ring experiment are shown by the red line. The reported uncertainty of the experimental data is larger than 15% due to the statistical and systematic errors [11]. In order to compare with the experimental data, the non-Maxwell–Boltzmann distribution over collision velocities was taken into considered as in previous studies [35–37]. Convolution was performed on the raw cross section using the parallel electron energy spread of $E_{\parallel} = 0.5$ meV and the transverse energy spread of $E_{\perp} = 25$ meV relevant to the ASTRID storage ring experiment [11]. The convolution washes out partially the structure of the drops at the vibrational thresholds. The convoluted cross sections are in an excellent agreement with the experimental curve below the vibrational threshold $\hbar\omega_3 = 0.21$ eV of the asymmetric CF stretching mode. The convoluted DR cross section of $CF_3^+$ is provided as supplementary data in 'convoluted $CF_3^+$ cross section.dat' file https://stacks.iop.org/PSST/31/045016/mmedia. The rate coefficients for DR and VE of CF3+ are provided as supplementary data in 'thermal_rate_DR.dat' and 'thermal_rate_VE.dat' files.

Thermally-averaged rate coefficients are evaluated from the cross sections by the standard formula

$$\alpha(T) = \frac{8\pi}{(2\pi k_{\rm b}T)^{3/2}} \int_0^\infty \sigma(E_{\rm el}) \exp\left(-\frac{E_{\rm el}}{k_{\rm b}T}\right) E_{\rm el}\, {\rm d}E_{\rm el}, \quad (10)$$

where $k_{\rm b}$ is the Boltzmann coefficient and $T$ is the temperature. Inserting equations (8) and (9) with the linear function of the probability $P_i$ to equation (10), the corresponding rate coefficients for VE and DR can be written as

$$\alpha_i^{\rm VE}(T) = \sqrt{\frac{2\pi}{k_{\rm b}T}} \frac{\hbar^2}{m^{3/2}} (a_i k_{\rm b}T + a_i\hbar\omega_i + b_i) \exp\left(-\frac{\hbar\omega_i}{k_{\rm b}T}\right), \quad (11)$$

and

$$\alpha^{\rm DR}(T) = \sqrt{\frac{2\pi}{k_{\rm b}T}} \frac{\hbar^2}{m^{3/2}} \times \sum_{i=1}^{4} \left[ (a_i k_{\rm b}T + b_i) \left(1 - \exp\left(-\frac{\hbar\omega_i}{k_{\rm b}T}\right)\right) - a_i\hbar\omega_i \exp\left(-\frac{\hbar\omega_i}{k_{\rm b}T}\right)\right]. \quad (12)$$

The computed DR rate coefficient is shown in figure 5. At 300 K, the coefficient is $1.39 \times 10^{-7}$ cm$^3$ s$^{-1}$.

We note here that the DR rate coefficient reported in the experimental paper as the fit $2.6 \times 10^{-7}(300\ {\rm K}/T)^{0.48}$ cm$^3$ s$^{-1}$ does not agree with the values obtained here. Because the theoretical and experimental cross sections, employed to produce the rate coefficients, agree with each other, it is possible that the fit is not accurate.

Figure 5 also shows rate coefficients for VE of all four modes by one quantum. As one can see (also evident in figure 3), the rate coefficient for excitation of the breathing mode is significantly smaller than for other modes. This is because the leading contribution to excitation of modes

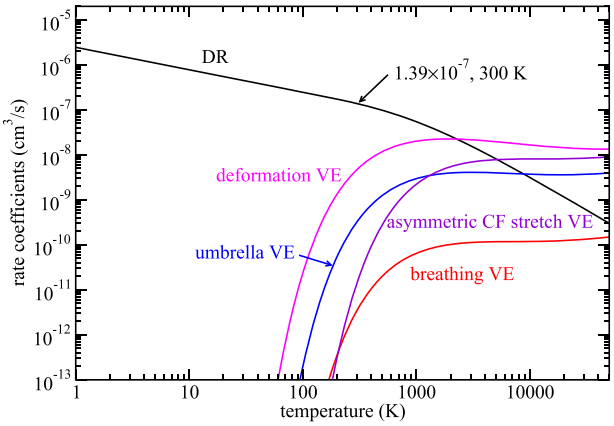


**Figure 5.** Computed VE and DR rate coefficients.

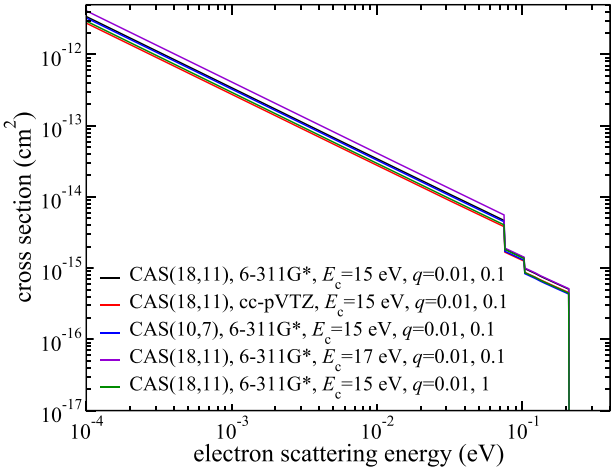


**Figure 6.** Assessment of the uncertainty of the present calculations of the DR cross section. Complete DR calculations were performed for five sets of parameters of the theoretical model: (1) CAS(18, 11), 6-311G*, $E_c = 15$ eV, $q = 0.01, 0.1$; (2) CAS(18, 11), cc-pVTZ, $E_c = 15$ eV, $q = 0.01, 0.1$; (3) CAS(10, 11), 6-311G*, $E_c = 15$ eV, $q = 0.01, 0.1$; (4) CAS(18, 11), 6-311G*, $E_c = 17$ eV, $q = 0.01, 0.1$; and (5) CAS(18, 11), 6-311G*, $E_c = 15$ eV, $q = 0.01, 1$.

2–4 is due to the variation of the dipole moment of the target ion, while for mode 1 (breathing) the dipole moment is zero for all normal mode displacements, so that the leading contribution to the VE probability is due to variation of the quadrupole moment of the ion and its polarizability. The contribution of the charge-quadrupole interaction and polarizability of the target to the excitation probabilities is significantly smaller than the effect of the dipole moment. Therefore, the rate coefficient for excitation of the breathing mode is significantly smaller than the coefficients for the other modes that are dipole-allowed.

Uncertainties of the present theoretical results are estimated by varying various parameters of the mode: the basis set, the CAS, the cutoff energy $E_c$, and the interval of normal coordinates $q$ used in calculations of derivatives of the $S$-matrix. Complete calculations of the DR cross section were performed for five sets of parameters (1) CAS(18, 11), 6-311G*, $E_c = 15$ eV, $q = 0.01, 0.1$; (2) CAS(18, 11), cc-pVTZ, $E_c = 15$ eV, $q = 0.01, 0.1$; (3) CAS(10, 11), 6-311G*, $E_c = 15$ eV, $q = 0.01, 0.1$; (4) CAS(18, 11), 6-311G*, $E_c = 17$ eV, $q = 0.01, 0.1$; and (5) CAS(18, 11), 6-311G*, $E_c = 15$ eV, $q = 0.01, 1$. The results of the five calculations are shown in figure 6. The uncertainty of the rates computed by (1) and (3) demonstrates a maximum value of about 20%.

## 4. Plasma etching implications

Plasma etching is one of the critical processes in the microelectronic industry [38, 39]. The ultimate goal of etching is to remove some material from surfaces with good controlled selectivity and anisotropy. Different mixtures of species can be used or involved in the process [40], such as electrons, $CF_3^+$ and $F^-$ ions, radicals of $CF_3$ and F, etc. Etch rate, etching selectivity, and anisotropy are controlled by concentrations of the species, which are determined by collisions in the gas phase and at the surface.

Many atomic and molecular collisions are involved in the formation of the etching plasma, such as elastic, excitation, ionization, recombination, and so on. Cross section data are of a vital importance to simulate the plasma accurately. Generally, relatively good cross section sets for elastic, excitation, ionization collisions are available either from experiments or calculations [41]. However, recombination cross sections are not widely available due to the lack of direct measurements. At present, some simple estimation based on the recombination rate is used instead, both in Monte Carlo [42–44] and fluid simulation [45]. $C_xF_y$ gases are widely used for plasma etching. The C:F ratio is one of the most important factors to affect the process. In discharges, the recombination process of electrons with $CF_3^+$ will affect the balance of different species in the etching plasma. Therefore, the DR cross section and rate coefficients obtained in this work will lead to more accurate plasma modeling. For Monte Carlo simulations, the cross section can be used directly. We expect some improvement of the results can be achieved both in PIC/MC [8, 46, 47] and fluid simulation [45]. This is especially important for pulsed plasma [48, 49], in which the plasma gradually decays and the temperature can change significantly.

## 5. Conclusions and discussions

In this study, we have computed cross sections for the VE and DR of $CF_3^+$ in collisions with low energy electrons. The employed theoretical approach combines the normal mode approximation, vibrational frame transformation, and $R$-matrix method. The rotational structure of the target ion was neglected, so that the obtained results should be viewed as averaged over the initial rotational states and summed over the final rotational states of the corresponding initial and final vibrational levels. The computed DR cross section agrees well with the experimental data from the ASTRID storage ring experiment. The obtained data are important for accurate modeling of the $CF_4$ etching plasma modeling.

The present theoretical approach accounts only for the indirect mechanism of DR and is valid only for scattering energies

below the vibrational threshold (0.21 eV) of the asymmetric CF stretching mode. At higher scattering energies, above 0.21 eV and below approximately 7 eV, the DR cross section is significantly smaller than at low energies, but not zero like in the present model. To model the DR process at energies 0.21–7 eV, one would need to include the effect of the Rydberg series converging to highly-excited vibrational levels. It is, in principle, possible to extend the model to these energies accounting for higher derivatives in the expansion of the scattering matrix along the normal mode coordinates. However, this theoretical development has not been made so far. At even higher energies, from approximately 7 eV to 12 eV, one would have to account for Rydberg resonances produced by excited electronic states. Again, it is, in principle, possible to extend the present model to account for these resonance. The broad resonance at around 8 eV in the experimental DR cross section is possibly caused by such Rydberg resonances associated with excited electronic states of the molecular ion. Some of the potential energy surfaces of these resonances must be dissociative so that they open the direct mechanism for the DR process at these energies. Although the cross section of the (direct and indirect) DR at higher energies is significantly smaller than at low energies, it is still comparable to the cross section of many other collisional processes taking place in a plasma environment. Hence, an extension of the method to higher scattering energies (up to 10 eV) is definitely needed and will be attempted in a further study.

## Acknowledgments

This work acknowledges the support from the National Science Foundation (Grant No. 2110279), the Thomas Jefferson Fund of the Office for Science and Technology of the Embassy of France in the United States, the National Natural Science Foundation of China (Grant Nos. 11775164, 11775090 and 12011530142), and the Fundamental Research Funds for the Central Universities (WUT: 2020IB023). It has also received funding from the program 'Accueil des chercheurs étrangers' of CentraleSupélec.

## Data availability statement

The data that support the findings of this study are available from the corresponding author upon reasonable request.

## ORCID iDs

Xianwu Jiang https://orcid.org/0000-0002-7605-8036
Ya Zhang https://orcid.org/0000-0003-0473-467X
Wei Jiang https://orcid.org/0000-0002-9394-585X
Mehdi Ayouz https://orcid.org/0000-0002-0447-5551
Viatcheslav Kokoouline https://orcid.org/0000-0002-9945-0858

## References

[1] Christophorou L G, Olthoff J K and Rao M V V S 1996 *J. Phys. Chem. Ref. Data* **25** 1341–88
[2] Kimura T and Ohe K 2002 *J. Appl. Phys.* **92** 1780–7
[3] Peko B L, Dyakov I V, Champion R L, Rao M V V S and Olthoff J K 1999 *Phys. Rev.* E **60** 7449
[4] Denpoh K and Nanbu K 2000 *Japan. J. Appl. Phys.* **39** 2804
[5] Li Z-C, Chang D-L, Li X-S, Bi Z-H, Lu W-Q, Xu Y, Zhu A-M and Wang Y-N 2010 *Phys. Plasmas* **17** 033501
[6] Zhang Y-R, Tinck S, Schepper P D, Wang Y-N and Bogaerts A 2015 *J. Vac. Sci. Technol.* A **33** 021310
[7] Kimura T and Noto M 2006 *J. Appl. Phys.* **100** 063303
[8] Georgieva V, Bogaerts A and Gijbels R 2004 *Phys. Rev.* E **69** 026406
[9] Samukawa S 2014 *Etching Gas* (New York: Wiley)
[10] Christophorou L G and Olthoff J K 1999 *J. Phys. Chem. Ref. Data* **28** 967–82
[11] Ehlerding A *et al* 2006 *J. Phys. B: At. Mol. Opt. Phys.* **39** 805
[12] Samukawa S, Mukai T and Noguchi K 1999 *Mater. Sci. Semicond. Process.* **2** 203–8
[13] Nakano T and Sugai H 1992 *Japan. J. Appl. Phys.* **31** 2919
[14] Sugai H 1995 *Contrib. Plasma Phys.* **35** 415–20
[15] Bartschat K and Kushner M J 2016 *Proc. Natl Acad. Sci. USA* **113** 7026–34
[16] Biondi M 1976 *Principles of Laser Plasmas* (New York: Wiley)
[17] Mantzaris N V, Boudouvis A and Gogolides E 1995 *J. Appl. Phys.* **77** 6169–80
[18] Angelova G, LeGarrec J L, Rebrion-Rowe C, Rowe B R, Novotny O and Mitchell J B A 2004 *J. Phys. B: At. Mol. Opt. Phys.* **37** 4135
[19] Fournier J A, Shuman N S, Melko J J, Ard S G and Viggiano A A 2013 *J. Chem. Phys.* **138** 154201
[20] Douguet N, Orel A, Mikhailov I, Schneider I F, Greene C H and Kokoouline V 2011 *J. Phys.: Conf. Ser.* **300** 012015
[21] Fonseca dos Santos S, Douguet N, Kokoouline V and Orel A E 2014 *J. Chem. Phys.* **140** 164308
[22] Kokoouline V, Ayouz M, Mezei J Z, Hassouni K and Schneider I F 2018 *Plasma Sources Sci. Technol.* **27** 115007
[23] Yuen C H, Ayouz M A, Balucani N, Ceccarelli C, Schneider I F and Kokoouline V 2019 *Mon. Not. R. Astron. Soc.* **484** 659–64
[24] Ayouz M A, Yuen C H, Balucani N, Ceccarelli C, Schneider I F and Kokoouline V 2019 *Mon. Not. R. Astron. Soc.* **490** 1325–31
[25] Pak Y and Woods R C 1997 *J. Chem. Phys.* **106** 6424–9
[26] Davydov A S 1976 *Quantum Mechanics* 2nd edn (Oxford: Pergamon)
[27] Werner H-J, Knowles P J, Knizia G, Manby F R and Schütz M 2012 *Wiley Interdiscip. Rev.-Comput. Mol. Sci.* **2** 242–53
[28] Dossmann H, Garcia G A, Nahon L, de Miranda B K C and Alcaraz C 2012 *J. Chem. Phys.* **136** 204304
[29] Forney D, Jacox M E and Irikura K K 1994 *J. Chem. Phys.* **101** 8290–6
[30] Halasinski T M, Godbout J T, Allison J and Leroi G E 1994 *J. Phys. Chem.* **98** 3930–2
[31] Tennyson J 2010 *Phys. Rep.* **491** 29–76
[32] Tennyson J, Brown D B, Munro J J, Rozum I, Varambhia H N and Vinci N 2007 Quantemol-N: an expert system for performing electron molecule collision calculations using the *R*-matrix method *J. Phys.: Conf. Ser.* **86** 012001
[33] Mikhaylov I A, Kokoouline V, Larson Å, Tonzani S and Greene C H 2006 *Phys. Rev.* A **74** 032707
[34] Wigner E P 1948 *Phys. Rev.* **73** 1002
[35] Kokoouline V and Greene C H 2005 *J. Phys.: Conf. Ser.* **4** 010

[36] Jiang X 2020 Hydrocarbon molecules databases for waste treatment applications *PhD Thesis* Université Paris-Saclay
[37] Jiang X, Forer J, Yuen C H, Ayouz M and Kokoouline V 2021 *Phys. Rev.* A **104** 042801
[38] Lieberman M A and Lichtenberg A J 2005 *Principles of Plasma Discharges and Materials Processing* (New York: Wiley)
[39] Makabe T and Petrovic Z L 2006 *Plasma Electronics: Applications in Microelectronic Device Fabrication* (Boca Raton, FL: CRC Press)
[40] Fridman A 2008 *Plasma Chemistry* (Cambridge: Cambridge University Press)
[41] Kurihara M, Petrovic Z L and Makabe T 2000 *J. Phys. D: Appl. Phys.* **33** 2146
[42] Nanbu K 2000 *IEEE Trans. Plasma Sci.* **28** 971–90
[43] Denpoh K and Nanbu K 1998 *J. Vac. Sci. Technol.* A **16** 1201–6
[44] Denpoh K and Nanbu K 2000 *Japan. J. Appl. Phys.* **39** 2804–8
[45] Rauf S and Kushner M J 1997 *J. Appl. Phys.* **82** 2805–13
[46] Georgieva V, Bogaerts A and Gijbels R 2003 *J. Appl. Phys.* **94** 3748–56
[47] Donkó Z and Petrović Z L 2006 *Japan. J. Appl. Phys.* **45** 8151
[48] Wang X-F, Jia W-Z, Song Y-H, Zhang Y-Y, Dai Z-L and Wang Y-N 2017 *Phys. Plasmas* **24** 113503
[49] Jia W-Z, Wang X-F, Song Y-H and Wang Y-N 2017 *J. Phys. D: Appl. Phys.* **50** 165206